RADIOLARIAN AGE AND LITHOSTRATIGRAPHY OF LATE CRETACEOUS PELAGIC SEDIMENTS OVERLYING BASALTIC EXTRUSIVE ROCKS, NORTHERN OMAN MOUNTAINS

Kousuke Hara ✉ and **Toshiyuki Kurihara**

Graduate School of Science and Technology, Niigata University, Japan.
✉ *Corresponding author, email: mournful.gecko.and.lively.newt@gmail.com*

Keywords: *Oman Ophiolite*, *ridge magmatism*, *extrusive lava*, *metalliferous sediments*, *pelagic sediments*, *Radiolaria, biostratigraphy*, *Cenomanian*, *Turonian*, *Late Cretaceous*.

ABSTRACT

A detailed radiolarian biostratigraphy of pelagic sediments overlying basaltic extrusive lavas of the Oman Ophiolite is reported for the type locality of the Suhaylah Formation near the Wadi Jizzi River, northern Oman Mountains. The extrusive lavas in the studied section are classified as V1 lava produced by mid-ocean-ridge magmatism. The sedimentary succession in the type section (ca. 18 m thick) is subdivided into three units (in stratigraphic order): metalliferous sediments (Unit 1), red mudstone intercalated with radiolarian chert (Unit 2), and micritic limestone (Unit 3).

The recovery of well-preserved radiolarians from all units led to the recognition of three distinctive assemblages: Assemblage A, obtained from metalliferous sediments and chert intercalations within red mudstone, could be correlated with the middle-late Cenomanian fauna; Assemblage B, recovered from red mudstone and chert, is assigned to the early Turonian, based on correlation with radiolarian occurrences across the Cenomanian-Turonian boundary; Assemblage C, recognized in micritic limestone, is broadly identified as Turonian-Coniacian.

The age of the Suhaylah Formation has previously been interpreted as early Cenomanian to Coniacian-Santonian; however, the revised age could be from late Cenomanian to Turonian-Coniacian. The estimated possible maximum age of metalliferous sediments (96.5-93.9 Ma) is in good agreement with high-precision U-Pb zircon dates of ophiolite crust attributed to ridge magmatism. The depositional age of the pelagic sediments clearly indicates that the ridge magmatism had ended by ca. 95.5 Ma.

INTRODUCTION

The Oman Ophiolite (or Semail Ophiolite) is part of the long chain of Tethyan ophiolites that extends from the western Mediterranean to Southeast Asia. This ophiolite, observable along the east coast of Oman and the United Arab Emirates, forms a huge thrust sheet that crops out for a length of 500 km and a width of approximately 80 km in the Oman Mountains. Many studies have been conducted to understand the genesis and emplacement process of this ancient oceanic lithosphere using systematic mapping, detailed petrological and geochemical analyses, and structural geology (e.g., Reinhardt, 1969; Glennie et al., 1973; 1974; Pearce et al., 1981; Lippard et al., 1986; Nicolas, 1989). These studies demonstrated that the ophiolite is the most complete preserved section of upper mantle to oceanic crust worldwide. The sequence is more than 15 km thick and consists of mantle peridotites, layered gabbros, sheeted dikes, and extrusive lavas. Geochronological studies using U-Pb dating of zircons from gabbros, tonalites, and trondhjemites indicate that the ophiolitic crust formed during the middle Cenomanian (96.0-95.5 Ma: Rioux et al., 2014).

The extrusive lavas in this ophiolite are geochemically diverse, including mid-ocean ridge basalt (MORB) or back-arc basin basalt (BABB), island-arc tholeiites, and calc-alkaline series lavas (e.g., Pearce et al., 1981; Alabaster et al., 1982; Ernewein et al., 1988; Umino et al., 1990; Ishikawa et al., 2002; Einaudi et al., 2003; Godard et al., 2003; A'Shaikh et al., 2005). Historically, these data have led to different interpretations of the tectonic setting of their formation. One hypothesis is that the ophiolite formed at a spreading axis above a subduction zone (e.g., Pearce et al., 1981; Alabaster et al., 1982); another is that it was generated at a mid-ocean ridge (e.g., Nicolas, 1989; Nicolas and Boudier, 2003). The presence of multiple generations of plutonism and volcanism within the mantle and crust has been also clearly demonstrated (e.g., Juteau et al., 1988; Adachi and Miyashita, 2003; Godard et al., 2006; Tamura and Arai, 2006; Goodenough et al., 2010). Although there is still no general agreement on the formation of ophiolites, an alternative proposal is the stepwise evolution of initial mid-ocean ridge magmatism and subsequent thrusting/subduction associated with primitive arc-like volcanism (e.g., Arai et al., 2006). This scenario is supported by recent volcanostratigraphic and geochemical studies (e.g., Kusano et al., 2012; 2014). In addition, high-precision U-Pb dating of gabbros, tonalites, and trondhjemites reveal that ridge magmatism and arc-like magmatism occurred during ca. 96.0-95.5 Ma and 95.5-95.0 Ma, respectively (Rioux et al., 2012; 2013; 2014), indicating rapid development of thrusting/subduction following formation of the ophiolite crust.

For age determination of the eruption of basaltic rocks within ophiolites, the biostratigraphic age of metalliferous sediments (umbers) and pelagic sediments overlying extrusive lavas is important (e.g., Robertson and Hudson, 1974; Robertson, 1975; Blome and Irwin, 1985). Tippit et al. (1981) provided a preliminary report on radiolarians possibly ranging in age from the early Cenomanian to the Coniacian-Santonian from sediments exposed around the Wadi Jizzi, northern Oman (Fig. 1). That study demonstrated the potential usefulness of radiolarians in constraining the timing of the termination of basaltic extrusive rocks; however, the work yielded limited information in terms of localities, sampling horizons, and the stratigraphic distribution and faunal composition of radiolarians, which are necessary for more accurate age determination. In addition, although the radiolarian chronology for the Late Cretaceous was greatly advanced in the 1980s and subsequently (e.g., O'Dogherty,

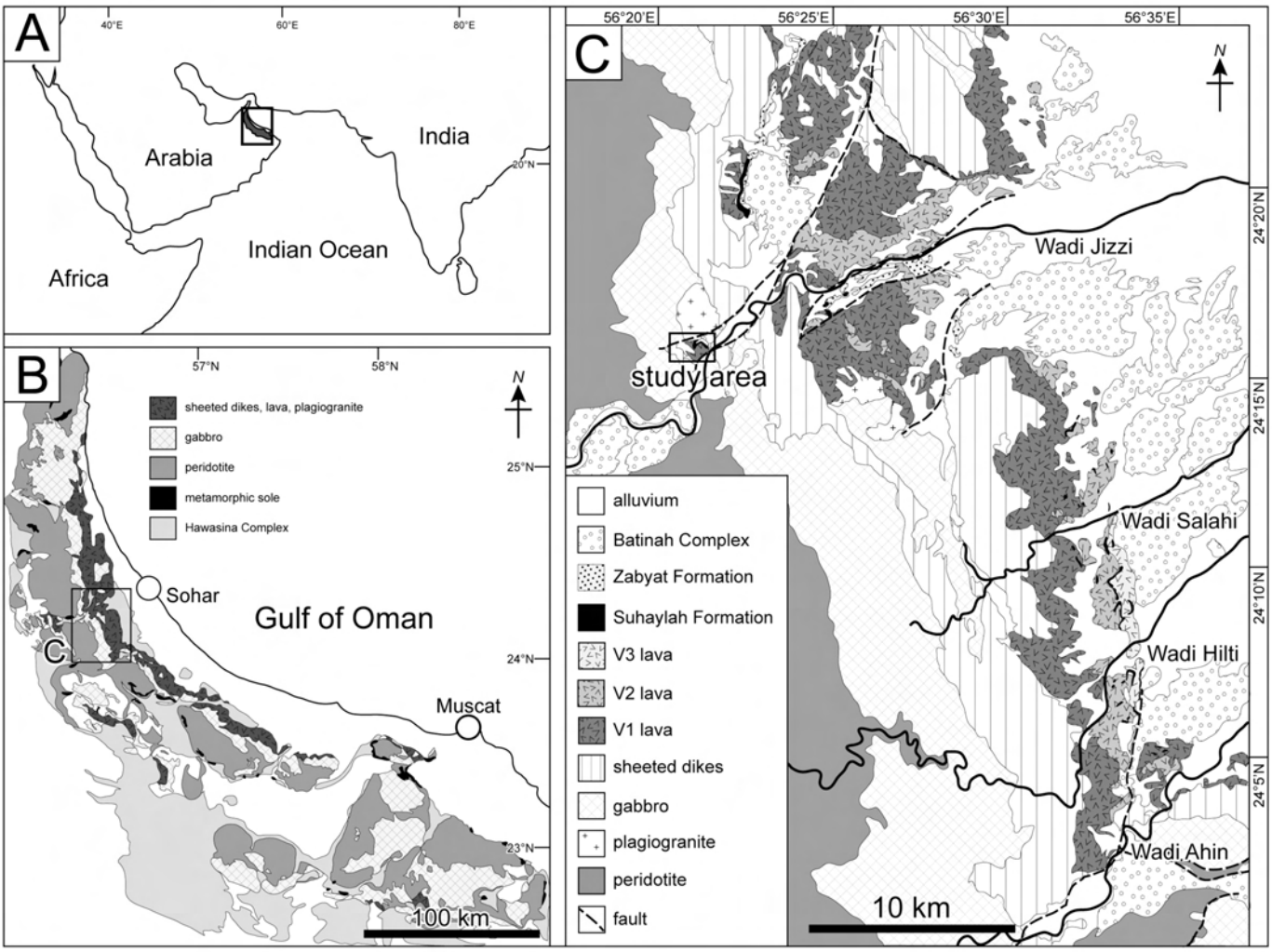

Fig. 1 - Index map showing the location of the study area (Wadi Jizzi area) in northern Oman. (A) Location of the Oman Ophiolite. (B) Distribution of ophiolitic rocks in Oman (modified from Nicolas et al., 2009). (C) Simplified geological map of the area west of Sohar. The base map is modified from Bishimetal Exploration Co. Ltd. (1987).

1994), there have been few applications of radiolarian dating to sediments overlying basaltic lavas.

In this study, we reexamined the stratigraphy, lithology, and radiolarian ages of metalliferous and pelagic sediments around the Wadi Jizzi, to clarify the nature of pelagic sedimentation around a spreading ridge and the history of volcanic activity of the ophiolite. We discovered abundant and diverse Late Cretaceous radiolarians from these sedimentary sequences. The obtained faunal assemblages are suitable for comparison with concurrent assemblages of the west Tethys. We describe the lithostratigraphy and faunal characteristics, and discuss the age of the radiolarian-bearing rocks and the eruption age of the basaltic lava in the study area.

REGIONAL GEOLOGIC FRAMEWORK

The extrusive lavas and overlying sedimentary sequence, consisting of metalliferous sediments, red mudstone with intercalated chert, and micritic limestone, are well exposed in the area about 40 km west of Sohar (Fig. 1), called the "Wadi Jizzi Zone" (Fleet and Robertson, 1980). Around this area, an almost complete oceanic crustal sequence is readily observable, which consists of harzburgites and dunites, layered gabbros, a sheeted-dike complex, and extrusive lavas (e.g., Lippard et al., 1986).

The extrusive lavas have been subdivided into five units: Geotimes, Lasail, Ally, CPX-phyric, and Salahi units on the basis of geochemical composition (e.g., Alabaster et al., 1982; Lippard et al., 1986; Ernewein et al., 1988). Of these, the Geotimes Unit directly overlies the sheeted-dike complex with a gradational contact (Lippard et al., 1986). Ernewein et al. (1988) summarized the subdivision of volcanic rocks and recognized that V1 (Geotimes Unit), which has a normal MORB (N-MORB)-like signature, was erupted around a spreading ridge and that V2 (Alley and CPX-phyric units) formed by intra-oceanic arc volcanism. In addition, thick lava flows of V3 (Salahi Unit), ascribed to intra-plate volcanism (Lippard et al., 1986; Ernewein et al., 1988), were emplaced onto pelagic sediments (Umino, 2012). Recently, Kusano et al. (2012) reexamined the stratigraphy of the volcanic units at Wadi Fizh, about 25 km north of Wadi Jizzi, based on their geochemical composition and stratigraphic relationships. This study subdivided the V1 extrusive rocks into four sub-units: the LV1a and LV1b (Lower V1 Sequence), MV1 (Middle V1 Sequence), and UV1 (Upper V1 Sequence).

Metalliferous and pelagic sediments commonly occur on lavas and at the boundaries between different volcanic units. The most thickly accumulated sediments (>15 m thick), which rest directly on the V1 lava (the 'lower' lava of the original description by Fleet and Robertson, 1980), were named the Suhaylah Formation (Fleet and Robertson, 1980; Woodcock and Robertson, 1982). The type section is located northwest of a small village (Suhaylah) near the Wadi Jizzi River (Fig. 2). Typical metalliferous sediments are dark purple-colored ferromanganiferous mudstone with amorphous Fe-Mn oxides. These metalliferous sediments change gradually to dark red-colored radiolarian mudstones with interbedded thin chert layers, which have higher silica and lower metal contents. The mudstone is conformably overlain by pelagic micritic limestone. Fleet and Robertson (1980) and Robertson and Fleet (1986) suggest that the metalliferous and pelagic sediments were accumulated on a horst-like topographic high by hydrothermal activity relatively far from a spreading center, and subsequent sedimentation of siliceous and calcareous ooze during gradual waning of the hydrothermal activity.

Glennie et al. (1974) reported a foraminifera (*Rotalipora* sp.) in lime-mudstone overlying pillow lava at Wadi Jizzi and assigned it to the Cenomanian. They also noted the occurrence of '*Globotruncana* species', including '*Globotruncana sigali*' and '*Globotruncana schneegansi*', in radiolarian chert and silicified lime-mudstone interbedded with pillow lava at Wadi Ragmi (Rajimi), located ~50 km north of Wadi Jizzi, and indicated a Coniacian age for these rocks. Tippit et al. (1981) conducted radiolarian-based biostratigraphic dating of metalliferous and pelagic sediments overlying the Geotimes Unit (V1 lava) and the Alley Unit (V2 lava). Based on the radiolarian biostratigraphic scheme of the late 1970s, they concluded that the age of the lower metalliferous sediments covering the V1 lava is early Cenomanian, whereas that of the upper micritic limestone is Coniacian-Santonian. Schaaf and Thomas (1986) reported a radiolarian fauna from chert overlying the ophiolite at Wadi Ragmi and interpreted its age as early Campanian; however, there are many unclear points about the stratigraphic positions of sampling horizons and faunal details. Beurrier et al. (1987) reported occurrences of possible Albian to Campanian radiolarians from sediments within the ophiolite over wide areas.

The Suhaylah Formation is overlain by the Zabyat Formation (Woodcock and Robertson, 1982; Robertson and Woodcock, 1983a) which consists of ophiolite debris, redeposited sandstone- to siltstone-sized volcaniclastic rocks, and pelagic mudstone. In the upper part of the ophiolite, the Batinah Complex (Woodcock and Robertson, 1982; Robertson and Woodcock, 1983b) widely overlies the extrusive lavas, the Suhaylah and Zabyat formations (see Figs. 1 and 2), and sometimes sheeted dikes with distinct erosional surfaces.

STUDY SECTIONS AND LITHOLOGY OF RADIOLARIAN-BEARING ROCKS

We conducted a radiolarian biostratigraphic study of the metalliferous and pelagic sediments of the Suhaylah Formation near Suhaylah Village, which is the type locality of this formation (Fleet and Robertson, 1980; Woodcock and Robertson, 1982) (Figs. 1 and 2). Fig. 2B shows the detailed distribution of the rocks of this formation and the locations of study sections (sections I to III). Tippit et al. (1981) reported radiolarians from a locality in the mapped area (Fig. 2B); however, the precise location of the analyzed section was not stated in their article.

The basaltic lavas that directly underlie the Suhaylah Formation are widely distributed in the study area. The lava is gray to greenish gray in color, and where altered is green

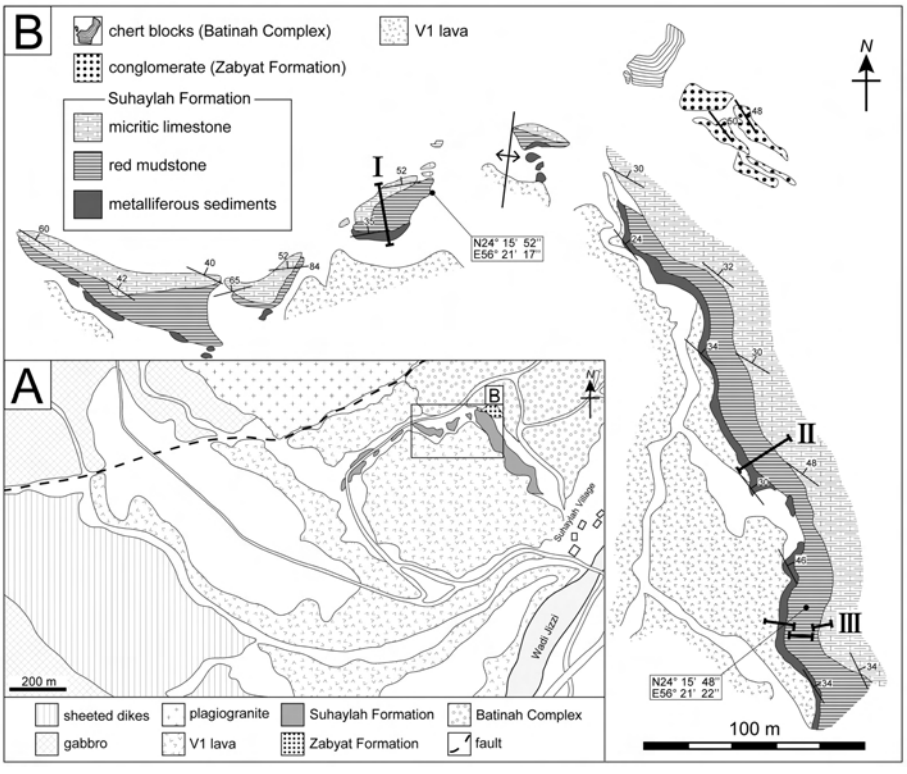

Fig. 2 - Index map showing the locations of examined sections (I, II, III). (A) Simplified geological map of the area northwest of Suhaylah Village. See Fig. 1 for the location of the mapped area. The base map is modified from Bishimetal Exploration Co. Ltd. (1987). (B) Geological map of the sampled area.

in color. Sheet lava dominates overall, and pillow lava is also seen locally. The basaltic lava of this area directly overlies sheeted dikes (Fig. 2A). All previous studies divided the basaltic lava of this area into the 'lower' lava, the Geotimes Unit, and the V1 sequence (Fleet and Robertson, 1980; Tippit et al., 1981; Robertson and Fleet, 1986; Bishimetal Exploration Co. Ltd., 1987; Kusano et al., 2014). The chemistry of the basaltic rocks that underlie the metalliferous sediments of the section analyzed herein allows classification of the rock as the Lower V1 Sequence of Kusano et al. (2012; Y. Kusano, pers. comm. in 2014).

In the uppermost part of the Suhaylah Formation in the study area, red siliceous mudstone is interbedded with thin volcanic sandstone layers and gradually changes upward into conglomerate of the Zabyat Formation, indicating a conformable relationship between the Suhaylah and Zabyat formations. The Batinah Complex, which consists of chert blocks within a volcaniclastic matrix, appears at the eastern end of the mapped area (Fig. 2A) and covers the conglomerate of the Zabyat Formation. Plagiogranite occurs in the north of the study section, in fault contact with the other units (Fig. 2A).

The sediments in the Suhaylah Formation, which have a maximum thickness of 18 m, are continuously exposed in three of the examined sections (sections I to III) and are subdivided into three lithologic units (units 1, 2, and 3 in ascending stratigraphic order; Figs. 3 and 4A). Unit 1 is composed mainly of metalliferous sediments, Unit 2 of red mudstone intercalated with chert, and Unit 3 of mainly micritic limestone.

Unit 1

Unit 1 consists mainly of metalliferous sediments interbedded with thin chert layers. The thickness of the unit ranges about 4 to 8 m. The basal portion that is in contact with the basaltic lava is characterized by a thin layer of reddish metalliferous sediments (Fig. 4B). According to Robertson and Fleet (1986), these sediments shows high SiO_2 values and are enriched in Fe_2O_3 rather than MnO. Above the basal layer, the sediments are very fine-grained and are commonly dark purple to dark red in color with a metallic luster. The sediments are enriched in Fe_2O_3 and MnO (Robertson and Fleet, 1986). Thin laminations within weakly stratified beds are commonly observed. The metallic luster is distinctive in the lower part and becomes less pro-

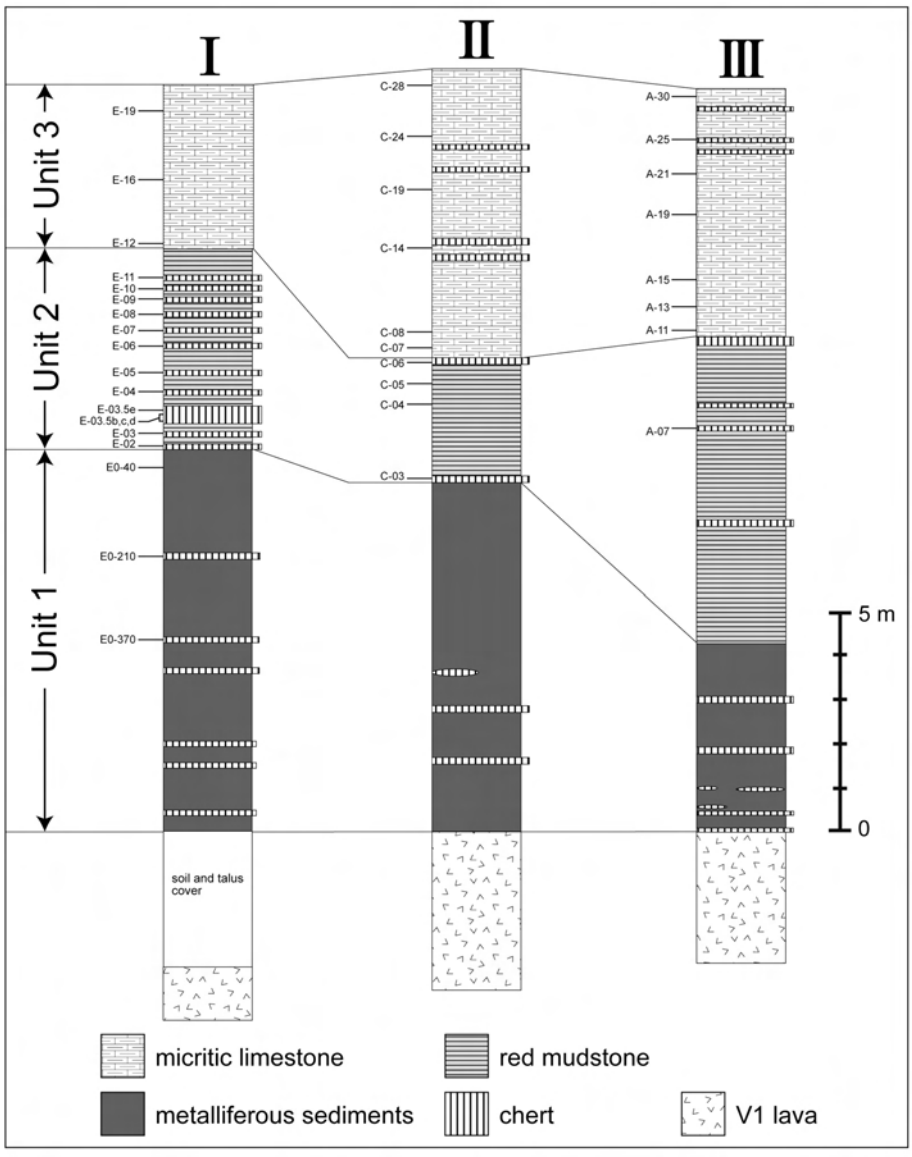

Fig. 3 - Selected lithostratigraphic columns measured within the Suhaylah outcrops including the sampled layers. See Fig. 2 for location details. Correlations indicated by solid lines are based on key lithostratigraphic boundaries.

nounced toward the upper part. In the lower part of this unit, hydrothermal chert occurs as thin interbeds (~ 20 cm thick) or nodular-shaped lenses within the metalliferous sediments (Fig. 4B). Although this chert contains rare radiolarian shells, the chert layers yield moderately preserved radiolarians at section I. The sediments in the upper part of this unit become more argillaceous and yield well-preserved radiolarians in section I (Figs. 3 and 5).

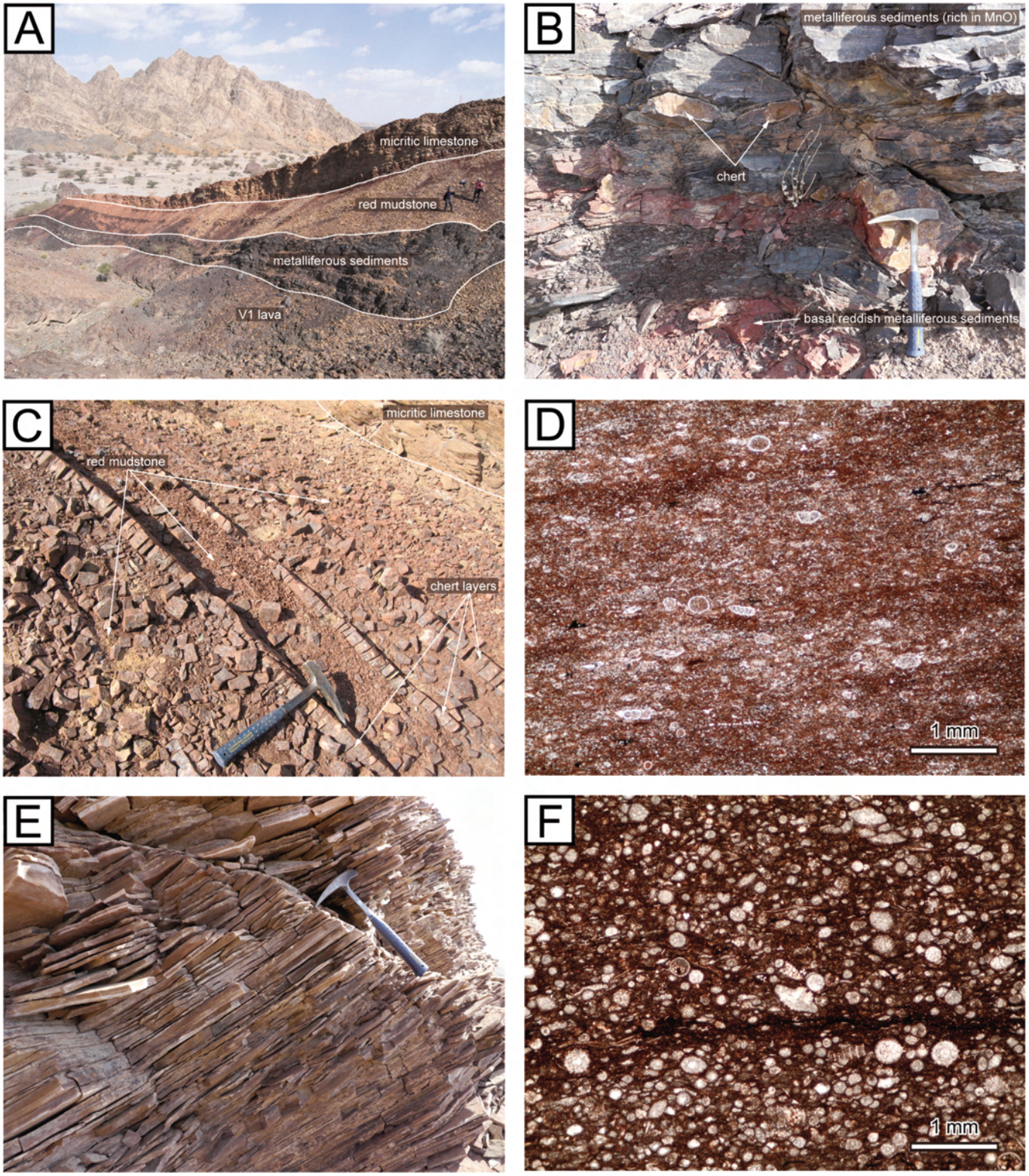

Fig. 4 - Outcrop photographs and photomicrographs showing the lithologies of pelagic sediments in the study area. (A) View of outcrops of the V1 lava and the Suhaylah Formation. (B) Metalliferous sediments and chert intercalations exposed at section III. (C) Alternating beds of red mudstone and radiolarian chert exposed at section I. (D) Photomicrograph of red mudstone exposed at section II (sample C-04) containing radiolarian skeletons. Plane-polarized light. (E) Micritic limestone exposed at section III. (F) Photomicrograph of micritic limestone at section II (sample C-08) containing many radiolarian skeletons. Plane-polarized light.

Unit 2

Unit 2 is composed mainly of radiolarian-bearing mudstone intercalated with radiolarian chert (Fig. 4C). This unit ranges in thickness about 2 to 7 m. The mudstone has a gradational contact with the metalliferous sediments of the underlying Unit 1. The mudstone is red in color and very fine-grained, without terrigenous crystalline particles such as quartz and feldspar. Well-preserved radiolarian tests occur sparsely in the matrix of clay minerals with hematite, although the originally spherical shells are sometimes preserved as ovoidal and compaction-flattened forms (Fig. 4D). In all sections, several radiolarian chert layers (5-10 cm thick) are intercalated with red mudstone. The chert contains numerous well-preserved radiolarian tests. At section I, the chert-layer intercalations are more common than in other sections, and therefore are suitable for studies of radiolarians. The rhythmic alternations of red mudstone and radiolarian chert are also observable in the upper part of this unit at section I (Fig. 4C).

Unit 3

This unit consists mainly of micritic limestone (Fig. 4E). The limestone changes gradually from the underlying red mudstone of Unit 2 through a thin transitional layer of muddy siliceous micrite. The limestone is thinly bedded (3 to 5 cm thick) and red-purple in color in the lower part and greenish-gray in the upper part. The matrix is fine-grained carbonate and clay minerals. Numerous well-preserved radiolarian shells without calcification can be observed within the matrix. Radiolarian tests, 80-350 μm in size, make up 50-80% by volume of the micritic limestone (Fig. 4F). The limestone of this unit is devoid of terrigenous crystalline particles and contains rare silicified foraminiferal remains. Several green radiolarian chert layers (5-15 cm thick) are intercalated with the upper parts of sections II and III. These layers contain abundant poorly preserved radiolarian tests.

RADIOLARIAN ASSEMBLAGES AND AGE ASSIGNMENTS

We collected more than 300 samples from metalliferous and pelagic sediments of the Suhaylah Formation to determine the depositional age. Radiolarians of siliceous samples (red mudstone and chert) were extracted using a standard hydrofluoric acid (HF) etching technique (Dumitrica, 1970; Pessagno and Newport, 1972). Samples of micritic limestone were soaked in a dilute hydrochloric acid (HCl) solution (ca. 38%) for about 24 hours to remove carbonate and were then treated with HF. Well-preserved radiolarians were recovered from 38 samples of metalliferous sediments, chert within metalliferous sediments, red mudstone, chert intercalated with red mudstone, and micritic limestone of sections I, II, and III (Fig. 3, Plates 1 and 2). Occurrence data of identified species from these samples are provided in Table 1. Detailed occurrences of the species in sections I to III are presented in Figs. 5, 6 and 7. The faunal change was determined at section I in detail. From the occurrence patterns, the species clearly make up three distinct assemblages (A to C): Assemblage A was recovered from metalliferous sediments and intercalated chert of Unit 1 (samples E0-370 to E0-40), and chert interbedded with red mudstone of Unit 2 (samples E-02 to E-03.5d, C-03, and A-07); Assemblage B was obtained from red mudstone and chert of Unit 2 (samples E-03.5e to E-11 and C-04 to C-06); Assemblage C was found in micritic limestone of Unit 3 (samples E-12 to E-19, C-07 to C-28, and A-11 to A-30). Below we describe the faunal characteristics and ages of these assemblages.

Assemblage A

Assemblage A is characterized by abundant *Thanarla pulchra* (Squinabol), *Thanarla veneta* (Squinabol), *Novixitus mclaughlini* (Pessagno), *Rhopalosyringium majuroense* Schaaf, *Holocryptocanium barbui* Dumitrica, *Holocryptocanium tuberculatum* Dumitrica, *Holocryptocanium* sp. A, *Guttacapsa biacuta* (Squinabol), *Guttacapsa gutta* (Squinabol), and *Hemicryptocapsa tuberosa* Dumitrica (Plate 1). Among these species, *T. pulchra*, *T. veneta*, *N. mclaughlini*, and *H. barbui* dominate the assemblage of the metalliferous sediments and chert of Unit 1 in section I. In contrast, *G. biacuta* and *G. gutta* are less abundant in the sediments of Unit 1 but they are abundant in the basal part of Unit 2, particularly in the chert. *Dactyliosphaera silviae* Squinabol, *Dactyliodiscus longispinus* (Squinabol), *Archaeodictyomitra montisserei* (Squinabol), *Rhopalosyringium petilum* (Foreman), *Pseudotheocampe* sp. A, and *Myllocercion* sp. are sparsely present in this assemblage. All species listed above disappear at horizons within Unit 2. *Dictyomitra multicostata* Zittel, *Hemicryptocapsa prepolyhedra* Dumitrica, *Hemicryptocapsa polyhedra* Dumitrica, *Pseudodictyomitra pseudomacrocephala* (Squinabol), *Pseudodictyomitra tiara* (Holmes), *Rhopalosyringium elegans* (Squinabol), *Rhopalosyringium hispidum* O'Dogherty, and *Stichomitra communis* Squinabol occur in assemblages A to C.

Of the species listed above, *T. pulchra* and *T. veneta* are well known from the Albian to Cenomanian worldwide, with last occurrences (LOs) at the top of the upper Cenomanian (Pessagno, 1977; O'Dogherty, 1994; Bragina, 2004; Musavu-Moussavou et al., 2007). According to the occurrence data of O'Dogherty (1994) that were obtained from the Northern Apennines (Italy) and the Betic Cordillera (Spain), the strata yielding Assemblage A of this study can be correlated with the Silviae Zone (*Dactyliosphaera silviae* Zone) of the uppermost early-late Cenomanian age, based on the occurrences of *D. silviae*, *Guttacapsa* species, *R. majuroense*, and *N. mclaughlini*. In this assemblage, *D. longispinus* was recovered from the lowest radiolarian-bearing horizon of Unit 1 of section I (sample E0-370). This species has been reported from Unitary Associations (UAs) 13 to 18 (Missilis Subzone to Biacuta Subzone) and latest Cenomanian (Musavu-Moussavou et al., 2007). *Rhopalosyringium petilum*, of which the UAs are in the range 14 to 18 (Anisa Subzone to Biacuta Subzone), are also present in this assemblage. Furthermore *G. biacuta* and *G. gutta* are commonly found in Assemblage A. The ranges of *G. biacuta* and *G. gutta* are restricted to UAs 17 to 19, corresponding to the upper part of the Spica Subzone (*Patellula spica* Subzone) and the whole Biacuta Subzone (*Guttacapsa biacuta* Subzone) of the Silviae Zone. This interval has been correlated to the middle to upper Cenomanian (Fig. 11 of O'Dogherty, 1994). In the present study, the LOs of *G. biacuta* and *G. gutta* are recognized in horizons (samples E-03 and E-03.5d, respectively) within Unit 2 of section I. Considering all data together, it appears reasonable to assign a middle to late Cenomanian age to Assemblage A, placing emphasis on the occurrences of *G. biacuta* and *G. gutta*.

In addition, the precise correlation between our studied section and the late Cenomanian to early Turonian stratigraphic intervals (around the Bonarelli level: BL) of Eu-

Table 1 - List of Late Cretaceous radiolarians from the Suhaylah outcrops (sections I, II, and III).

Section	III							II									I																			
Lithologic unit	2	3						2				3					1	2														3				
Samples / Species	A-07	A-11	A-13	A-15	A-19	A-21	A-25	A-30	C-03	C-04	C-05	C-06	C-07	C-08	C-14	C-19	C-24	C-28	E0-370	E0-210	E0-40	E-02	E-03	E-03.5b	E-03.5c	E-03.5d	E-03.5e	E-04	E-05	E-06	E-07	E-08	E-09	E-10	E-11	E-12	E-16	E-19
Assemblage	A	C						A	B			C					A									B									C		
Acaeniotyle rebellis		●	●	●	●								●			●	●	●																			
Acastea diaphorogona			●										●	●																								●
Alievium superbum		●	●	●	●	●	●	●		●	●		●		●	●	●	●																		●		●
Amphipternis sp. cf. *A. stocki*		●	●	●	●	●	●	●							●		●						●					●		●						●	●	●
Annikaella omanensis		●	●	●	●	●	●	●					●		●	●	●	●																		●	●	●
Archaeodictyomitra montisserei	●																		●	●	●	●	●															
Archaeodictyomitra vulgaris		●			●		●	●		●	●				●	●	●	●											●			●			●		●	●
Archaeospongoprunum andersoni			●										●			●	●	●																				
Archaeospongoprunum cortinaensis				●	●			●					●	●	●		●	●																	●		●	
Archaeospongoprunum stocktonensis														●	●		●																		●			●
Crucella cachensis			●	●		●		●		●	●		●	●		●	●	●										●							●	●	●	
Dactyliodiscus longispinus																			●																			
Dactyliosphaera silviae																			●	●	●	●	●															
Diacanthocapsa ovoidea																																●						●
Dictyomitra formosa		●	●	●				●		●	●		●	●	●	●	●	●														●	●		●	●	●
Dictyomitra multicostata		●	●	●	●	●	●	●		●	●		●	●	●	●	●	●						●	●				●		●	●					●
Eostichomitra sp. A			●	●						●				●	●		●	●									●	●	●	●	●	●	●					
Foremanina schona			●	●	●	●		●					●	●	●	●	●	●																		●	●	
Guttacapsa biacuta	●																		●	●	●	●	●															
Guttacapsa gutta																			●	●		●		●	●	●												
Hemicryptocapsa polyhedra		●	●	●	●	●	●	●		●				●	●	●	●	●			●			●	●	●	●		●	●		●	●			●		
Hemicryptocapsa prepolyhedra							●	●		●									●	●				●	●	●												
Hemicryptocapsa tuberosa	●																			●		●	●															
Holocryptocanium barbui																				●	●																	
Holocryptocanium tuberculatum																			●	●	●	●		●	●	●												
Holocryptocanium sp. A																			●	●		●		●	●	●												
Myllocercion valgus		●		●			●	●							●	●	●																			●	●	
Myllocercion sp.																			●		●	●	●															
Novixitus mclaughlini																			●	●	●				●													
Patellula ecliptica					●	●		●							●																							●
Patellula euessceei			●	●		●																																
Patellula helios					●		●	●					●																							●		
Patellula verteroensis			●		●	●		●					●		●	●	●	●																			●	●
Pessagnobrachia fabianii		●	●		●			●										●																				
Praeconocaryomma californiaensis			●	●	●	●		●		●	●		●	●	●	●	●	●																●		●		
Praeconocaryomma lipmanae			●			●								●		●	●																			●		
Praeconocaryomma universa			●		●						●			●	●		●	●																		●	●	
Pseudoaulophacus putahensis			●		●		●	●							●																					●	●	
Pseudodictyomitra pseudomacrocephala									●									●	●	●	●			●	●													
Pseudodictyomitra tiara		●	●				●	●		●	●					●	●	●	●	●	●			●	●		●		●					●	●	●	●	●
Pseudodictyomitra sp. A		●	●	●	●	●		●		●			●	●	●	●	●	●																	●	●	●	●
Pseudodictyomitra sp. B		●	●	●	●							●	●	●	●	●	●	●																		●	●	
Pseudotheocampe urna						●	●	●						●			●	●											●									●
Pseudotheocampe sp. A																			●	●	●																	
Rhopalosyringium elegans			●			●										●			●	●	●	●		●	●	●	●										●	
Rhopalosyringium hispidum							●																	●			●			●	●		●					
Rhopalosyringium majuroense																			●	●	●	●	●															
Rhopalosyringium petilum																				●	●	●	●															
Rhopalosyringium scissum		●	●	●	●	●	●	●		●	●		●	●	●	●	●	●									●	●	●	●	●	●	●	●	●	●	●	●
Rhopalosyringium sp. A		●	●	●	●	●	●			●	●		●	●	●	●	●	●										●	●				●	●	●	●	●	
Sandovaleila hastatus			●	●												●																				●		
Stichomitra communis	●								●			●			●		●		●	●	●	●	●	●				●	●			●	●	●	●	●		
Stichomitra manifesta		●																●																			●	
Thanarla pulchra	●																		●	●	●	●																
Thanarla veneta	●																		●	●	●				●													
Triactoma hexeris				●						●	●		●	●	●																		●					
Xitus spicularius	●	●	●	●	●	●	●	●		●	●				●	●	●	●														●				●	●

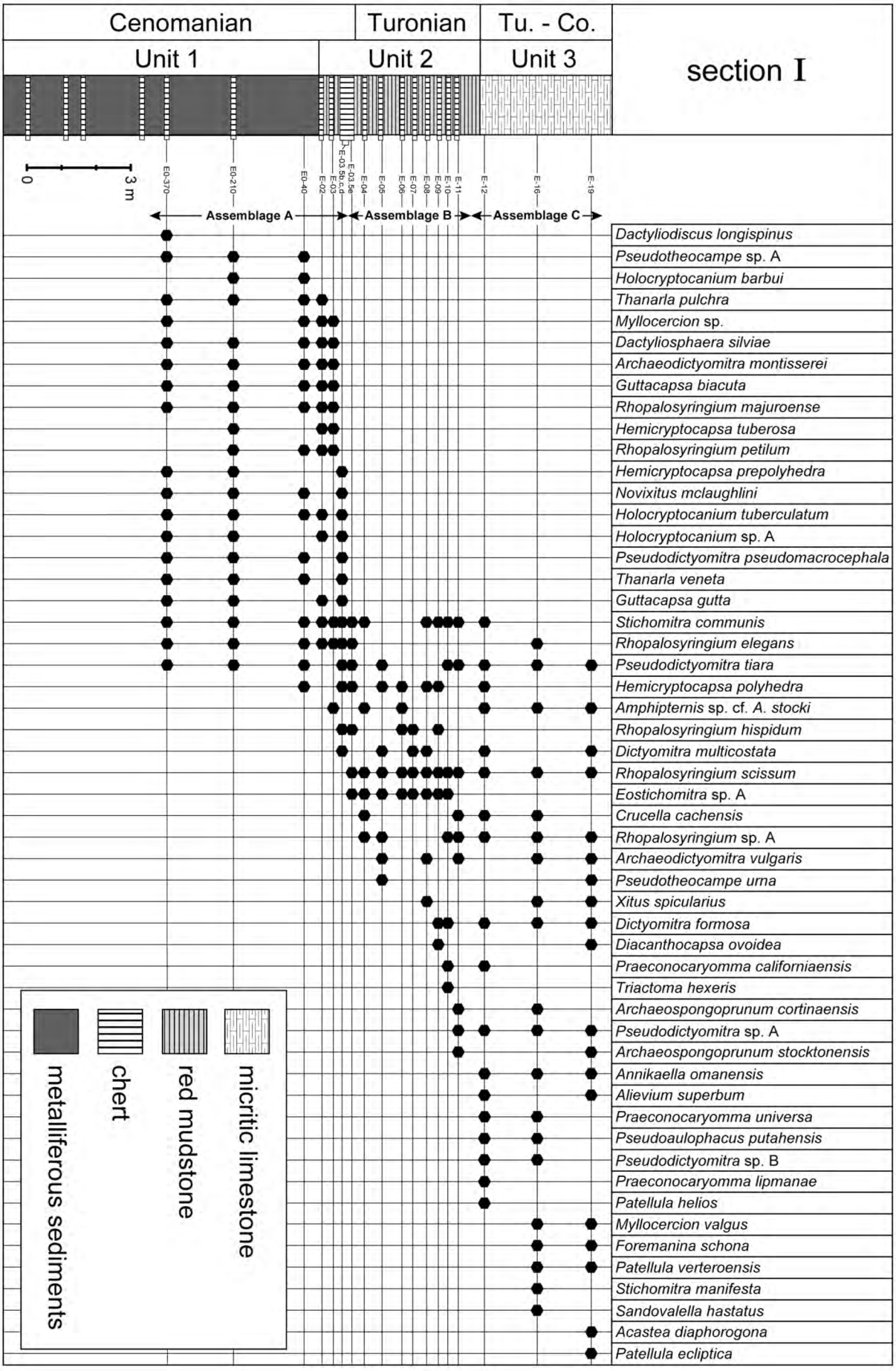

Fig. 5 - Occurrence of Late Cretaceous radiolarians in section I. Tu.: Turonian, Co.: Coniacian.

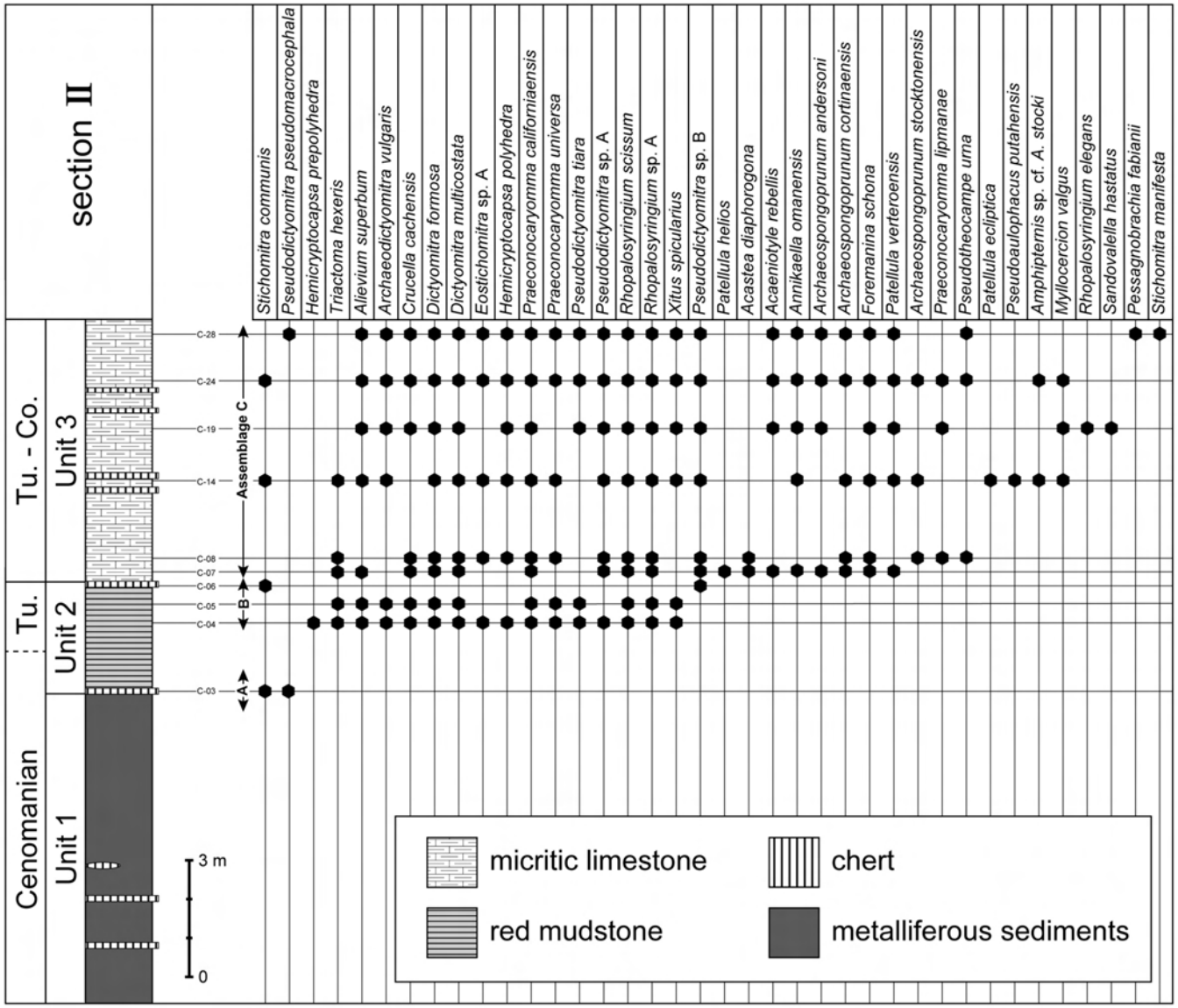

Fig. 6 - Occurrence of Late Cretaceous radiolarians in section II. Tu.: Turonian, Co.: Coniacian.

rope can provide an upper age limit for Assemblage A (Fig. 8). In this interval, the late Cenomanian oceanic anoxic event (OAE2) is a well-known geological event characterized by widespread deposition of organic-rich marine sediments, associated with a large perturbation of the carbon cycle (e.g., Schlanger and Jenkyns, 1976; Arthur et al., 1988). Many radiolarian studies have been conducted on the BL in terms of paleoenvironmental changes and radiolarian response during the OAE2 (e.g., Erbacher, 1994; Bąk, 2011). Musavu-Moussavou et al. (2007) examined the detailed radiolarian biostratigraphy across the BL of the Gubbio section, Italy, which is the one of the representative sections of the OAE2 (e.g., Tsikos et al., 2004; Wagreich et al., 2008). This section contains bituminous black mudstone and shale alternating with green-gray silty shale, radiolarian-rich mudstone, and silty sandstone, and is assigned to the latest Cenomanian (*Whiteinella archaeocretacea* Zone). Musavu-Moussavou et al. (2007) compiled the stratigraphic ranges of radiolarians across the BL from previous studies (Marcucci Passerini et al., 1991; Erbacher, 1994; Erbacher and Thurow, 1997; O'Dogherty, 1994; Gallicchio et al., 1996; Salvini and Marcucci Passerini, 1998). In Gubbio, the LOs of *G. biacuta*, *G. gutta*, and *R. majuroense* were recognized in the lower part of the BL (sample BL 1/02 of Musavu-Moussavou et al., 2007). In our section I, the LOs of *G. biacuta* and *R. majuroense* are recognized in the horizon of sample E-03. The LO horizon of *G. gutta* is sample E-03.5d. Based on the correlation of the LO horizon of *G. gutta*, the uppermost part yielding Assemblage A (basal part of Unit 2) is assigned to the latest Cenomanian (Fig. 8).

Assemblage B

Assemblage B is characterized by the abundance of *Rhopalosyringium scissum* O'Dogherty, *Dictyomitra formosa* Squinabol, *Dictyomitra multicostata* Zittel, *Hemicryptocapsa polyhedra* Dumitrica, *Stichomitra communis* Squinabol, *Eostichomitra* sp. A, and *Alievium superbum* (Squin-

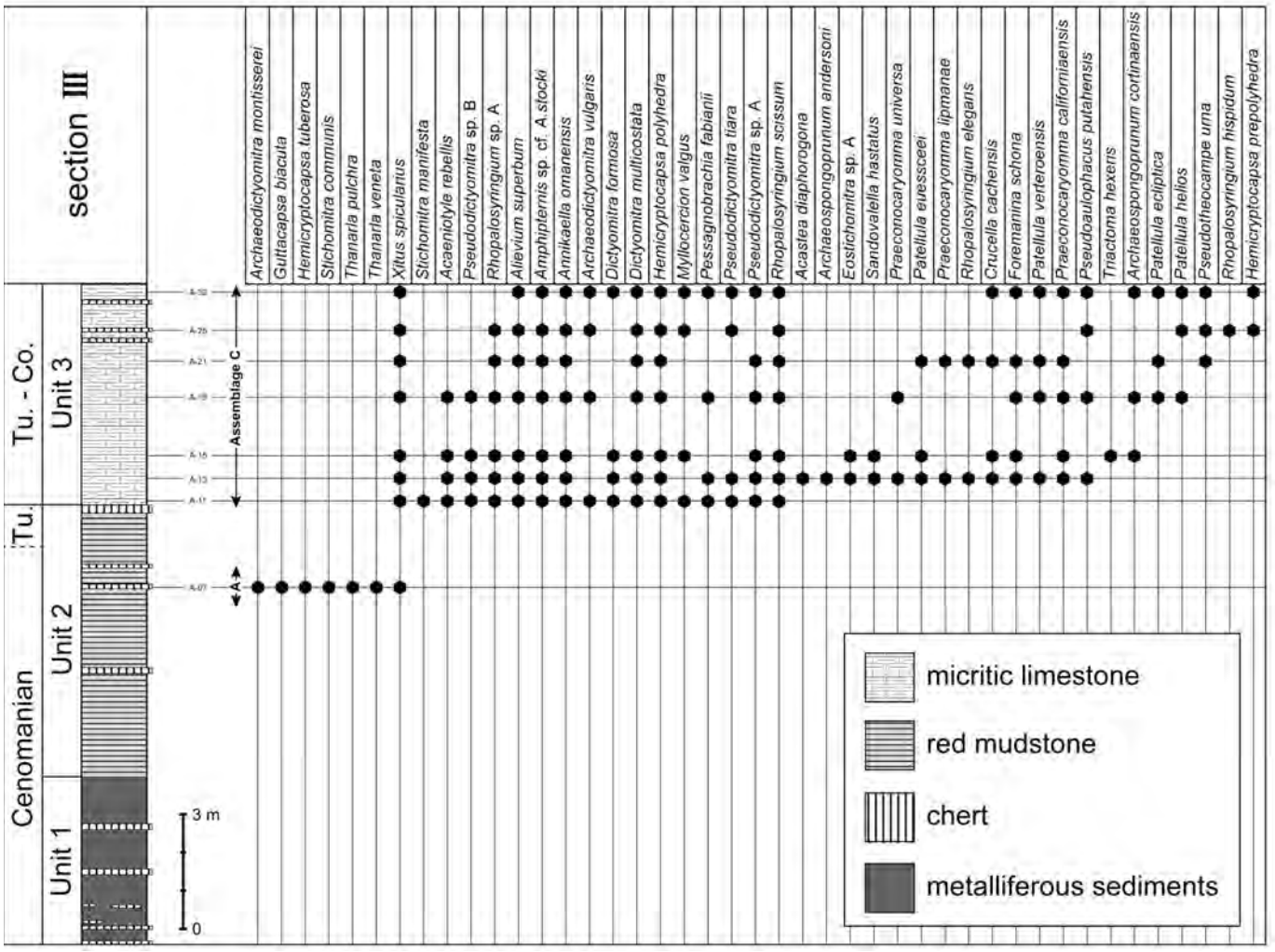

Fig. 7 - Occurrence of Late Cretaceous radiolarians in section III. Tu.: Turonian, Co.: Coniacian.

abol) (Plate 2). *Crucella cachensis* Pessagno, *Praeconocaryomma californiaensis* Pessagno, and *Praeconocaryomma universa* Pessagno are also present. *Pseudotheocampe urna* (Foreman) begins to appear in the chert interbedded within red mudstone of Unit 2. In this assemblage, *Rhopalosyringium scissum* is abundant in all analyzed sections and has its first occurrence (FO) in sample E-03.5e (ca. 10 cm above E-03.5d, which yielded Assemblage A) in section I (Figs. 5 and 8).

To determine the age of Assemblage B, we mainly follow the radiolarian studies of O'Dogherty (1994) and Musavu-Moussavou et al. (2007). O'Dogherty (1994) established the Superbum Zone (*Alievium superbum* Zone) for the Turonian. The FOs of *A. superbum* and other species such as *R. scissum* and *C. cachensis* have been reported as being at the base of this zone. The UAs of these species are in the range 20 to 21, indicating a Turonian age.

Musavu-Moussavou et al. (2007) recognized the FOs of *A. superbum*, *H. polyhedra*, and *C. cachensis* in the interval of the BL and placed the base of the Superbum Zone in the latemost Cenomanian (within the *W. archaeocretacea* Zone). The FO of *R. scissum* was recognized in the limestone several tens of centimeters above the BL (sample BTT 566 of Musavu-Moussavou et al., 2007; Figs. 5 and 8). *Dictyomitra multicostata* also first appeared in the limestone overlying the BL (sample BTT 564 of Musavu-Moussavou et al., 2007). In the Gubbio section, the Cenomanian-Turonian boundary deduced from the $\delta^{13}C$ profile and the biostratigraphic marker (the calcareous nannofossil *Quadrum gartneri* Prins and Perch-Nielsen) was placed ca. 1 m above the stratigraphic top of the BL (Tsikos et al., 2004). The FOs of *R. scissum* and *D. multicostata* in the Gubbio section are thus considered to be very close to the base of the Turonian. In the Suhaylah Formation, the FO of *R. scissum*, which is a potential biostratigraphic marker for the base of the Turonian, was confirmed at the horizon of sample E-03.5e. Based on the correlation between the radiolarian occurrences of the Gubbio section and the section analyzed in this study (section I), the stratigraphic interval from sample E-03.5e to E-04 at section could be considered to contain the C-T boundary (Fig. 8). Considering all the data together, we conclude that the age of Assemblage B is early Turonian.

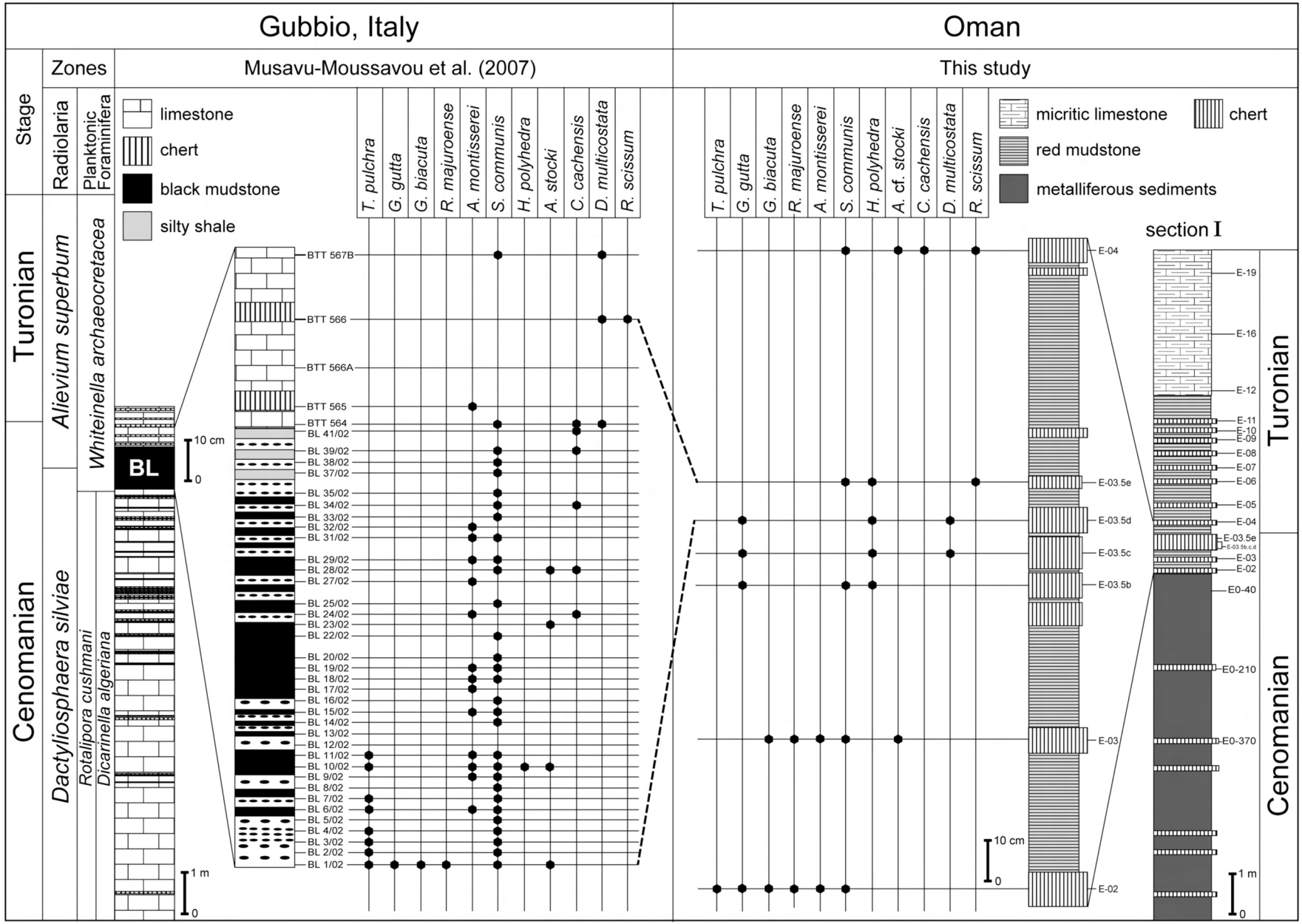

Fig. 8 - Correlation of the upper Cenomanian and Turonian between section I and the strata across the Bonarelli level (BL) in Gubbio, Italy (Musavu-Moussavou et al., 2007), based on radiolarian occurrences. The position of the Cenomanian-Turonian boundary in the Gubbio section is after Tsikos et al. (2004), who placed the level at ca. 1 m above the stratigraphic top of the BL. Broken lines indicate correlations based on key biohorizons: the last occurrence of *Guttacapsa gutta* (Squinabol) and the first occurrence of *Rhopalosyringium scissum* O'Dogherty.

Assemblage C

Assemblage C is characterized by the FOs of *Annikaella omanensis* De Wever, Bourdillon-de Grissac, and Beurrier, *Myllocercion valgus* (De Wever, Bourdillon-de Grissac, and Beurrier), *Foremanina schona* Empson-Morin, *Patellula verteroensis* (Pessagno), *Patellula ecliptica* O'Dogherty, *Patellula helios* (Squinabol), *Praeconocaryomma lipmanae* Pessagno, and *Pseudoaulophacus putahensis* Pessagno. In addition to these species, the following are also abundant: *Rhopalosyringium scissum* O'Dogherty, *Hemicryptocapsa polyhedra* Dumitrica, *Dictyomitra formosa* Squinabol, *Dictyomitra multicostata* Zittel, *Pseudodictyomitra* sp. A, *Pseudodictyomitra* sp. B, *Pseudotheocampe urna* (Foreman), *Amphipternis* sp. cf. *A. stocki* (Campbell and Clark), *Alievium superbum* (Squinabol), *Crucella cachensis* Pessagno, *Praeconocaryomma californiaensis* Pessagno, and *Praeconocaryomma universa* Pessagno (Plate 2). The LO of *Pseudodictyomitra pseudomacrocephala* (Squinabol) is recognized in sample C-28 from near the top of the Suhaylah Formation in section II (Figs. 3 and 6; Table 1; Fig. 29 of Plate 1).

This assemblage contains typical Turonian species such as *R. scissum*, *H. polyhedra*, *A. superbum*, and *C. cachensis* (e.g., O'Dogherty, 1994; Musavu-Moussavou et al., 2007). Considering the stratigraphic relationship to Assemblage B (early Turonian), it is reasonable to conclude that the age of the basal micritic limestone of Unit 3, which yields Assemblage C, is within the Turonian, because the limestone changes gradually from the underlying red mudstone of Unit 2 that contains Assemblage B. However, Assemblage C contains some species previously known to occur from the Coniacian onward. For example, *A. omanensis* is present abundantly in this assemblage, and is considered to be Santonian (De Wever et al., 1988) or late Coniacian to late Santonian in age (O'Dogherty et al., 2009). *Foremanina schona* has been reported from the Campanian (Empson-Morin, 1981; Urquhart and Banner, 1994; Moix et al., 2009) and *M. valgus* from the Santonian-Campanian (De Wever et al., 1988). This combination of species makes the age of the assemblage unclear; however, as a similar example to Assemblage C, Dumitrica et al. (1997) reported a Late Cretaceous radiolarian assemblage containing *A. omanensis* and *M. valgus* from the Masirah ophiolite of Oman, and noted that that assemblage possessed many species in common with the early Turonian assemblage described by O'Dogherty (1994). Robin et al. (2010) also reported *A. omanensis* in assemblage with typical Turonian species such as *H. polyhedra* from deep-water sediments in Iran (Pichakun nappes). We conducted research on the radiolarians of the micritic limestone by checking over 3,000 specimens, using SEM identifications. As a result, Assemblage C did not contain typical index species of Santonian to Campanian age, such as *Dictyomitra koslovae* Foreman, *Amphipyndax pseudoconulus* (Pessagno), *Amphipyndax tylotus* Foreman, and *Pseudoaulophacus floresensis* Pessagno (e.g., Hollis and Kimura, 2001).

For age constraints on Assemblage C, the occurrence of *P. pseudomacrocephala* at the top of the studied section indicates that the upper age limit of this assemblage is approximately within the Turonian (Pessagno, 1977; O'Dogherty, 1994; Bragina, 2004). Anyway according to Bandini et al. (2006), *P. pseudomacrocephala* has not been reported from later than the Coniacian. In conclusion, the age of Assemblage C is broadly determined as Turonian-Coniacian in the present study.

DISCUSSION

Revision of the biostratigraphic age of the Suhaylah Formation

Until now, the main evidence for the age of the Suhaylah Formation was the radiolarian faunas reported by Tippit et al. (1981). Herein we examined this fauna based on the current biostratigraphic scheme and determine the age of the formation based on our new radiolarian data.

Tippit et al. (1981) reported the following species from metalliferous sediments (sample 173) overlying the Geotimes Unit (V1 lava) in a location near Suhaylah (exact position not provided) in our mapped area (Fig. 2): *Quinquecapsularia spinosa* Pessagno, *Pseudodictyomitra pseudomacrocephala* (Squinabol), *Thanarla pulchra* (Squinabol), *Thanarla veneta* (Squinabol), *Hemicryptocapsa prepolyhedra* Dumitrica, *Holocryptocanium tuberculatum* Dumitrica, and *Holocryptocanium geysersensis* Pessagno. Based on the occurrences of these species, they assigned the sediments to the early Cenomanian. From micritic limestone underlain by metalliferous sediments and red radiolarian mudstone, *Hemicryptocapsa polyhedra* Dumitrica, *Crucella cachensis* Pessagno, *Praeconocaryomma universa* Pessagno, *Dictyomitra formosa* Squinabol, *Dictyomitra duodecimcostata* (Squinabol), and *Archaeospongoprunum rumseyense* Pessagno were recovered. The authors indicated the age of this fauna as Coniacian to Santonian. In addition, Tippit et al. (1981) noted the occurrence of planktonic foraminifera that are assigned to the '*Marginotruncana helvetica* Assemblage Zone (*Marginotruncana sigali* Subzone)' of Pessagno (1969) from the upper part of the red radiolarian mudstone (corresponding to the upper part of Unit 2 in our study), indicating the early Turonian, although species names and photographs were not provided in their study. Based on their data, the age of the Suhaylah Formation ranges from the early Cenomanian, through the early Turonian, to the Coniacian-Santonian.

In the present study, Assemblage A included almost all the species reported in sample 173 of Tippit et al. (1981). According to O'Dogherty (1994), these species have Albian to Turonian age ranges, and the co-occurrence of *T. pulchra*, *T. veneta*, and *H. prepolyhedra* indicates UAs 17 to 19 (middle to late Cenomanian). As mentioned above, our biostratigraphic result for Assemblage A indicates that the metalliferous sediments of Unit 1, corresponding to the basal part of the Suhaylah Formation, can be assigned a middle to late Cenomanian age; in other words, the chronological reinterpretation of the previously reported fauna is consistent with the results of our reexamination of the biostratigraphy. Tippit et al. (1981) described the red radiolarian mudstone as yielding early Turonian foraminifera; however, it is difficult to reexamine this foraminiferal age because no photographs of fossils were provided. This lithology corresponds to Unit 2 in our lithostratigraphic subdivision, which has an age range of latest Cenomanian to early Turonian across the possible C-T boundary. This finding is also consistent with the description of Tippit et al. (1981).

The fauna from micritic limestone reported by Tippit et al. (1981), which was assigned a Coniacian-Santonian age, has some species in common with our Assemblage C, but typical index species of Santonian age are not present, such as *Dictyomitra koslovae* Foreman and *Pseudoaulophacus floresensis* Pessagno (e.g., Hollis and Kimura, 2001). Based on the age determination of Assemblage C, the age of the micritic limestone is within the Turonian-Coniacian.

In conclusion, the biostratigraphy of the studied sections indicates that the Suhaylah Formation, from the basal metalliferous sediments and overlying pelagic red mudstone to micritic limestone, ranges in age from middle-late Cenomanian to Turonian-Coniacian, on the basis of the ages assigned to the three radiolarian assemblages in the sections. According to Gradstein et al. (2012), the numerical ages of the base of the middle Cenomanian and the top of the Coniacian are 96.5 Ma and 86.3 Ma, respectively. Therefore, the biostratigraphic results indicate that the time interval represented by the Suhaylah Formation is a maximum of approximately 10 Myr.

Significance for age constraints on the V1 lava

For ophiolite studies, it is critical to understand the formation of the oceanic crustal features of ophiolites and their emplacement process along the time-dimension established from radiometric and biostratigraphic ages (e.g., Hacker and Gnos, 1997). From this point of view, the maximum age of the metalliferous and pelagic sediments immediately above the V1 lava provides information about the approximate termination age of the mid-ocean-ridge magmatism; this can provide age constraints on the changes in tectonic setting indicated by different basaltic lava units, each of which has its own geochemical characteristics. The comparison between the U-Pb isotopic age of crustal rocks (trondhjemites) within the ophiolite and the biostratigraphic age of the overlying sediments (Tippit et al., 1981) was first discussed by Tilton et al. (1981). Both ages were in accordance with each other at that time, although the precision of the age data could be improved. Tippit et al. (1981) concluded that the volcanic activity of a ridge-axis, represented by the Geotimes Unit (V1 lava), occurred in the early Cenomanian; however, we revised the age of the metalliferous sediments to middle-late Cenomanian, meaning the estimated maximum possible age is 96.5 Ma. After the study of Tilton et al. (1981), the chronology of trondhjemites related to the ridge magmatism was investigated by Warren et al. (2005), indicating an age of ca. 95 Ma; however, these younger ages were suggested to reflect post-crystallization Pb-loss (Rioux et al., 2012; Searle et al., 2015).

High-precision U-Pb zircon dating has been conducted by Rioux et al. (2012; 2013; 2014) on gabbros, tonalites, and trondhjemites exposed (from south to north) in the Wadi Tayin, Samail, Rustaq, and Haylayn areas, south and west of Muscat, and the Fizh area, northwest of Sohar. According to Rioux et al. (2013; 2014), the rocks fall into two groups in terms of their structural positions, dates, and isotopic composition: the older group, dated at ca. 96.0-95.5 Ma (middle Cenomanian), is attributed to ridge magmatism, whereas the younger group (ca. 95.5-95.0 Ma) is related to post-ridge magmatism. The V1 lava is interpreted as the extrusive component of the former group (Lippard et al., 1986; Ernewein et al., 1988; Rioux et al., 2013). Although there is generally some difficulty in comparing radiometric and biostratigraphic ages for the Mesozoic, our detailed radiolarian study allows a substantial discussion, as follows. We estimate 96.5-93.9 Ma (middle-late Cenomanian) as the maximum possible age of the metalliferous sediments, based on the age of Assemblage A. This estimated age overlaps with the U-Pb zircon age of gabbroic crustal rocks formed by ridge magmatism (ca. 96.0-95.5 Ma: Rioux et al., 2013; 2014). In addition, the base of strata yielding Assemblage B within Unit 2 lies across the possible C-T boundary. It is worth of note that the C-T boundary is well constrained by $^{40}Ar/^{39}Ar$ ages from bentonites as 93.9 Ma (Gradstein et al., 2012). All that can be said with certainty is that the V1 lava generated by ridge magmatism has an age not younger than 95.5 Ma and therefore there had been sufficient time for the continuous deposition of a 10-m thickness of metalliferous and pelagic sediments upon the lava (Fig. 3). Thus, we conclude that the radiolarian age of the overlying sediments on the V1 lava is in good agreement with the U-Pb zircon dates of the ophiolite crusts that formed by ridge magmatism, and considering all the data we could indicate a late Cenomanian age for Assemblage A.

Recent studies have described details of the volcanostratigraphy and geochemical features of other volcanic units formed by post-ridge magmatism (Umino, 2012; Kusano et al., 2014). These volcanic rocks are closely associated with pelagic sediments that contain radiolarians (Kurihara and Hara, 2012). The results of this study, in combination with the volcano-stratigraphy and possible future reinvestigations of radiolarian biostratigraphy across a much wider area, will provide essential information on the age and formation of the Oman Ophiolite.

CONCLUSIONS

This paper reports new lithostratigraphic and biostratigraphic data for the type locality of the Suhaylah Formation, which consists of metalliferous and pelagic sediments overlying basaltic extrusive lavas (V1 lava) of the Oman Ophiolite and crops out near the Wadi Jizzi River, about 40 km west of Sohar, northern Oman Mountains. The results of our high-resolution radiolarian biostratigraphic study provide age constraints on the termination of the V1 lava attributed to ridge magmatism. The main findings of this study are summarized as follows.

(1) As described in previous studies, the Suhaylah Formation consists mainly of lower metalliferous sediments (umbers) that grade into overlying red mudstone intercalated with radiolarian chert, which is in turn overlain by upper micritic limestone. These strata preserve an essentially continuous record from the first deposition of metalliferous sediments related to hydrothermal activity around a ridge, to the subsequent pelagic sedimentation of red mudstone with chert and micritic limestone slightly farther from the ridge. All lithologies contain moderately to well-preserved radiolarians that allow age determinations.

(2) Three distinctive middle-late Cenomanian to Turonian-Coniacian radiolarian assemblages occur in the studied sections. The lowest assemblage, of middle to late Cenomanian age, was obtained from metalliferous sediments and chert intercalations within red mudstone. The early Turonian assemblage was recovered from red mudstone and chert. Based on the correlation between the radiolarian occurrences around the Bonarelli level at the Gubbio section, Italy, and our analyzed section, the stratigraphic interval around the lower part of red mudstone is considered to lie across the possible Cenomanian-Turonian boundary. The upper assemblage that was obtained from micritic limestone is assigned to the Turonian-Coniacian.

(3) In previous studies, the Suhaylah Formation was dated as early Cenomanian to Coniacian-Santonian. We revised the age of this formation to middle-late Cenomanian to Turonian-Coniacian, a maximum time interval of nearly 10 Myr, based on the radiolarian biostratigraphy. In addition, a

synthesis of our biostratigraphic result and the U-Pb dates of the ophiolite crust indicates that the Suhaylah Formation could be deposited during the late Cenomanian to Turonian-Coniacian.

(4) The radiolarian age of the sediments overlying the V1 lava is consistent with the high-precision U-Pb zircon age of crustal rocks formed by ridge magmatism. The depositional age of the pelagic sediments indicates that ridge magmatism had ended by ca. 95.5 Ma.

ACKNOWLEDGEMENTS

We thank the Ministry of Commerce and Industry, Directorate General of Minerals in Oman for facilitating our fieldwork. We express our thanks to S. Miyashita, Y. Kusano, S. Umino, E. Takazawa, Y. Adachi, and N. Tuchiya for fruitful discussions and for their kind support during our field surveys. Thanks are also due to Marco Chiari for his editorial handling of the paper. We are grateful to U. Kagan Tekin and an anonymous reviewer for their constructive reviews. This work was supported by JSPS Institutional Program for Young Researcher Overseas Visits 'Structure and Formation of the Oceanic Crust-Mantle System: Preparation for Mohole' and KAKENHI Grant No. 26400499.

REFERENCES

Adachi Y. and Miyashita S., 2003. Geology and petrology of the plutonic complexes in the Wadi Fizh area: Multiple magmatic events and segment structure in the northern Oman ophiolite. Geochem. Geophys. Geosyst., 4: 8619, doi: 10.1029/2001GC000272.

Alabaster T., Pearce J.A. and Malpas J., 1982. The volcanic stratigraphy and petrogenesis of the Oman ophiolite complex. Contrib. Mineral. Petrol., 81: 168-183.

Arai S., Kadoshima K. and Morishita T., 2006. Widespread arc-related melting in the mantle section of the northern Oman ophiolite as inferred from detrital chromian spinels. J. Geol. Soc. London, 163: 869-879.

Arthur M.A., Dean W.E. and Pratt L.M., 1988. Geochemical and climatic effects of increased marine organic carbon burial at the Cenomanian/Turonian boundary. Nature, 335: 714-717.

A'Shaikh D., Miyashita S. and Matsueda H., 2005. The petrological and geochemical characteristics of an ophiolite volcanic suite from the Ghayth area of Oman. J. Mineral. Petrol. Sci., 100: 202-220.

Bąk M., 2011. Tethyan radiolarians at the Cenomanian-Turonian Anoxic Event from the Apennines (Umbria-Marche) and the Outer Carpathians: palaeoecological and palaeoenvironmental implications. Studia Geol. Polonica, 134: 5-279.

Bandini A.N., Baumgartner, P.O. and Caron M., 2006. Turonian radiolarians from Karnezeika, Argolis Peninsula, Peloponnesus (Greece). Ecl. Geol. Helv., 99, Suppl. 1: S1-S20.

Beurrier M., Bourdillon-de Grissac C., De Wever P. and Lescuyer J.-L., 1987. Biostratigraphie des radiolarites associées aux volcanites ophiolitiques de la nappe de Samail (Sultanat d'Oman): conséquences tectogénétiques. C.R. Acad. Sci. Paris, Série II, 304: 907-910.

Bishimetal Exploration Co. Ltd., 1987. Geological Map of Wadi Bani Umar, sheet NG40-14E-II, scale 1:50,000 with explanatory notes. Ministr. Petr. Miner., Muscat.

Blome C.D. and Irwin W.P., 1985. Equivalent radiolarian ages from ophiolitic terranes of Cyprus and Oman. Geology, 13: 401-404.

Bragina L.G., 2004. Cenomanian-Turonian radiolarians of northern Turkey and the Crimean Mountains. Paleont. J., 38: 325-456.

De Wever P., Bourdillon-de Grissac C. and Beurrier M., 1988. Radiolaires Sénoniens de la nappe de Samail (Oman). Rev. Micropaléont., 31: 166-179.

Dumitrica P., 1970, Cryptocephalic and cryptothoracic Nassellaria in some Mesozoic deposits of Romania. Rev. Roum. Geol. Geophys. Geogr., 14: 45-124.

Dumitrica P., Immenhauser A. and Dumitrica-Jud R., 1997. Mesozoic radiolarian biostratigraphy from Masirah Ophiolite, Sultanate of Oman. Part I: Middle Triassic, uppermost Jurassic and Lower Cretaceous spumellarians and multisegmented nassellarians. Bull. Nat. Mus. Nat. Sci., 9: 1-106.

Einaudi F., Godard M., Pezard P., Cochemé J.-J., Coulon C., Brewer T. and Harvey P., 2003. Magmatic cycles and formation of the upper oceanic crust at spreading centers: Geochemical study of a continuous extrusive section in the Oman ophiolite. Geochem. Geophys. Geosyst., 4: 8608, doi:10.1029/2002GC000362.

Empson-Morin K.M., 1981. Campanian Radiolaria from DSDP Site 313, Mid-Pacific Mountains. Micropaleontology, 27: 249-292.

Erbacher J., 1994. Entwicklung und Paläoozeanographie mittelkretazischer Radiolarien der westlichen Tethys (Italien) und des Nordatlantiks. Tübinger Mikropal. Mitt., 12: 1-120.

Erbacher J. and Thurow J., 1997. Influence of oceanic anoxic events on the evolution of mid-Cretaceous radiolaria in the North Atlantic and western Tethys. Mar. Micropal., 30: 139-158.

Ernewein M., Pflumio C. and Whitechurch H., 1988. The death of an accretion zone as evidenced by the magmatic history of the Sumail ophiolite (Oman). Tectonophysics, 151: 247-274.

Fleet A.J. and Robertson A.H.F., 1980. Ocean-ridge metalliferous and pelagic sediments of the Semail Nappe, Oman. J. Geol. Soc. London, 137: 403-422.

Gallicchio S., Marcucci M., Pieri P., Premoli Silva I., Sabato L. and Salvini G., 1996. Stratigraphical data from a Cretaceous claystones sequence of the "Argille Varicolori" in the Southern Apennines (Basilicata, Italy). Palaeopelagos, 6: 261-272.

Glennie K.W., Boeuf M.G.A., Hughes Clarke M.W., Moody-Stuart M., Pilaar W.F.H. and Reinhardt B.M., 1973. Late Cretaceous nappes in Oman Mountains and their geologic evolution. Bull. Am. Ass. Petrol. Geol., 57: 5-27.

Glennie K.W., Boeuf M.G.A., Hughes Clarke M.W., Moody-Stuart M., Pilaar, W.F.H. and Reinhardt B.M., 1974. Geology of the Oman Mountains. Verhand. Koninkl. Neder. Geol. Mijnb. Genoot., 31: 423 pp.

Godard M., Bosch D. and Einaudi F., 2006. A MORB source for low-Ti magmatism in the Semail ophiolite. Chem. Geol., 234: 58-78.

Godard M., Dautria J.-M. and Perrin M., 2003. Geochemical variability of the Oman ophiolite lavas: Relationship with spatial distribution and paleomagnetic directions. Geochem. Geophys. Geosyst., 4: 8609, doi:10.1029/2002GC000452.

Goodenough K.M., Styles M.T., Schofield D., Thomas R.J., Crowley Q.C., Lilly R.M., McKervey J., Stephenson D. and Carney J.N., 2010. Architecture of the Oman-UAE ophiolite: evidence for a multi-phase magmatic history. Arab. J. Geosci., 3: 439-458.

Gradstein F.M., Ogg J.G., Schmitz M.D. and Ogg G., 2012. The Geologic Time Scale 2012, Volume 2. Elsevier, Amsterdam, 1144 pp.

Hacker B.R. and Gnos E., 1997. The conundrum of samail: explaining the metamorphic history. Tectonophysics, 279: 215-226.

Hollis C.J. and Kimura K., 2001. A unified radiolarian zonation for the Late Cretaceous and Paleocene of Japan. Micropaleontology, 47: 235-255.

Ishikawa T., Nagaishi K. and Umino S., 2002. Boninitic volcanism in the Oman ophiolite: Implications for thermal condition during transition from spreading ridge to arc. Geology, 30: 899-902.

Juteau T., Ernewein M., Reuber I., Whitechurch H. and Dahl R., 1988. Duality of magmatism in the plutonic sequence of the Sumail Nappe, Oman. Tectonophysics, 151: 107-135.

Kurihara T. and Hara K., 2012. Late Cretaceous radiolarians from pelagic sedimentary rocks on the basaltic extrusive rocks (V2 lava) of the Oman Ophiolite. Proceed. of 13th INTERRAD, Radiolaria Newsl., 28: 230-231.

Kusano Y., Adachi Y., Miyashita S. and Umino S., 2012. Lava accretion system around mid-ocean ridges: Volcanic stratigraphy in the Wadi Fizh area, northern Oman ophiolite. Geochem. Geophys. Geosyst., 13: Q05012, doi: 10.1029/2011GC004006.

Kusano Y., Hayashi M., Adachi Y., Umino S. and Miyashita S., 2014. Evolution of volcanism and magmatism during initial arc stage: constraints on the tectonic setting of the Oman Ophiolite. In: H.R. Rollinson, M.P. Searle, I.A. Abbasi, A. Al-Lazki and M.H. Al Kindi (Eds.), Tectonic evolution of the Oman Mountains. Geol. Soc. London Spec. Publ., 392: 177-193.

Lippard S.J., Shelton A.W. and Gass I.G., 1986. The Ophiolite of Northern Oman. Geol. Soc. London Mem., 11: 178 pp.

Marcucci Passerini M., Bettini P., Dainelli J. and Sirugo A., 1991. The "Bonarelli Horizon" in the central Apennines (Italy): radiolarian biostratigraphy. Cretaceous Res., 12: 321-331.

Moix P., Goričan Š. and Marcoux J., 2009. First evidence of Campanian radiolarians in Turkey and implications for the tectonic setting of the Upper Antalya Nappes. Creta. Res., 30: 952-960.

Musavu-Moussavou B., Danelian T., Baudin F., Coccioni R. and Fröhlich F., 2007. The Radiolarian biotic response during OAE2. A high-resolution study across the Bonarelli level at Bottaccione (Gubbio, Italy). Rev. micropaléont., 50: 253-287.

Nicolas A., 1989. Structures of Ophiolites and Dynamics of Oceanic Lithosphere. Kluwer Acad. Publ., Dordrecht, 367 pp.

Nicolas A. and Boudier F., 2003. Where ophiolites come from and what they tell us. In: Y. Dilek and S. Newcomb (Eds.), Ophiolite Concept and the Evolution of Geological Thought. Geol. Soc. Am. Spec. Pap., 373: 137-152.

Nicolas A., Boudier F. and France L., 2009. Subsidence in magma chamber and the development of magmatic foliation in Oman ophiolite gabbros. Earth Planet. Sci. Lett., 284: 76-87.

O'Dogherty L., 1994. Biochronology and paleontology of Mid-Cretaceous radiolarians from northern Apennines (Italy) and Betic Cordillera (Spain). Mém. Géol., Lausanne, 21: 1-415.

O'Dogherty L., Carter E.S., Dumitrica P., Goričan Š., De Wever P., Bandini A.N., Baumgartner P.O. and Matsuoka A., 2009. Catalogue of Mesozoic radiolarian genera. Part 2: Jurassic-Cretaceous. Geodiversitas, 31: 271-356.

Pearce J.A., Alabaster T., Shelton A.W. and Searle M.P., 1981. The Oman ophiolite as a Cretaceous arc-basin complex: evidence and implications. Philos. Trans. Royal Soc. London, A 300: 299-317.

Pessagno Jr. E.A., 1969. Upper Cretaceous stratigraphy of the Western Gulf Coast Area of México, Texas, and Arkansas. Geol. Soc. Am. Mem., 111: 1-139.

Pessagno Jr. E.A., 1977. Lower Cretaceous radiolarian biostratigraphy of the Great Valley Sequence and Franciscan Complex, California Coast Ranges. Cushman Foundation for Foraminiferal Research, Spec. Publ., 15: 1-87.

Pessagno Jr. E.A. and Newport R.L., 1972. A technique for extracting Radiolaria from radiolarian cherts. Micropaleontology, 18: 231-234.

Reinhardt B.M., 1969. On the genesis and emplacement of ophiolites in the Oman Mountains geosyncline. Schweiz. Min. Petrol. Mitt., 49: 1-39.

Rioux M., Bowring S., Garber J., Kelemen P., Searle M., Miyashita S. and Adachi Y., 2014. The development of subduction below the Oman-UAE ophiolite: Detailed temporal constraints from high precision U-Pb Zircon geochronology. AGU Fall Meeting 2014, Abstr., V51F-03.

Rioux M., Bowring S., Kelemen P., Gordon S., Dudás F. and Miller R., 2012. Rapid crustal accretion and magma assimilation in the Oman-U.A.E. ophiolite: High precision U-Pb zircon geochronology of the gabbroic crust. J. Geophys. Res., 117: B07201, doi:10.1029/2012JB009273.

Rioux M., Bowring S., Kelemen P., Gordon S., Miller R. and Dudás F., 2013. Tectonic development of the Samail ophiolite: High-precision U-Pb zircon geochronology and Sm-Nd isotopic constraints on crustal growth and emplacement. J. Geophys. Res., Solid Earth, 118: 2085-2101, doi:10.1002/jgrb.50139, 2013.

Robertson A.H.F., 1975. Cyprus umbers: basalt-sediment relationships on a Mesozoic ocean ridge. J. Geol. Soc. London, 131: 511-531.

Robertson A.H.F. and Fleet A.J., 1986. Geochemistry and palaeo-oceanography of metalliferous and pelagic sediments from the Late Cretaceous Oman ophiolite. Mar. Petrol. Geol., 3: 315-337.

Robertson A.H.F. and Hudson J.D., 1974. Pelagic sediments in the Cretaceous and Tertiary history of the Troodos Massif, Cyprus. In: K.J. Hsü and H.C. Jenkyns (Eds.), Pelagic sediments: on land and under the Sea. Spec. Publ. Int. Ass. Sedim., 1: 403-436.

Robertson A.H.F. and Woodcock N.H., 1983a. Zabyat Formation, Semail Nappe, Oman: sedimentation on to an emplacing ophiolite. Sedimentology, 30: 105-116.

Robertson A.H.F. and Woodcock N.H., 1983b. Genesis of the Batinah mélange above the Semail ophiolite, Oman. J. Struct. Geol., 5: 1-17.

Robin C., Goričan Š., Guillocheau F., Razin P., Dromart G. and Mosaffa H., 2010. Mesozoic deep-water carbonate deposits from the southern Tethyan passive margin in Iran (Pichakun nappes, Neyriz area): biostratigraphy, facies sedimentology and sequence stratigraphy. In: P. Leturmy and C. Robin (Eds.), Tectonic and stratigraphic evolution of Zagros and Makran during the Mesozoic-Cenozoic. Geol. Soc. London Spec. Publ., 330: 179-210.

Salvini G. and Marcucci Passerini M., 1998. The radiolarian assemblages of the Bonarelli Horizon in the Umbria-Marche Apennines and Southern Alps, Italy. Creta. Res., 19: 777-804.

Schaaf A. and Thomas V., 1986. Les Radiolaires campaniens du Wadi Ragmi (nappe de Semail, Oman): un nouveau repère chronologique de l'obduction omanaise. C.R. Acad. Sci. Paris, Série II, 303: 1593-1598.

Schlanger S.O. and Jenkyns H.C., 1976. Cretaceous oceanic anoxic events: causes and consequences. Geol. Mijnb., 55: 179-184.

Searle M.P., Waters D.J., Garber J.M., Rioux M., Cherry A.G. and Ambrose T.K., 2015. Structure and metamorphism beneath the obducting Oman ophiolite: Evidence from the Bani Hamid granulites, northern Oman mountains. Geosphere, 11: doi: 10.1130/GES01199.1.

Tamura A. and Arai S., 2006. Harzburgite-dunite-orthopyroxenite suite as a record of supra-subduction zone setting for the Oman ophiolite mantle. Lithos, 90: 43-56.

Tilton G.R., Hopson C.A. and Wright J.E., 1981. Uranium-lead isotopic ages of the Samail ophiolite, Oman, with applications to Tethyan ocean ridge tectonics. J. Geophys. Res., 86: 2763-2775.

Tippit P.R., Pessagno Jr. E.A. and Smewing J.D., 1981. The biostratigraphy of sediments in the volcanic unit of the Samail ophiolite. J. Geophys. Res., 86: 2756-2762.

Tsikos H., Jenkyns H.C., Walsworth-Bell B., Petrizzo M.R., Forster A., Kolonic S., Erba E., Premoli Silva I., Baas M., Wagner T. and Sinninghe Damsté J.S., 2004. Carbon-isotope stratigraphy recorded by the Cenomanian-Turonian Oceanic Anoxic Event: correlation and implications based on three key localities. J. Geol. Soc. London, 161: 711-719.

Umino S., 2012. Emplacement mechanism of off-axis large submarine lava field from the Oman Ophiolite. J. Geophys. Res., 117: B11210, doi: 10.1029/2012JB009198.

Umino S., Yanai S., Jaman A.R., Nakamura Y. and Iiyama J.T., 1990. The transition from spreading to subduction: evidence from the Semail ophiolite, northern Oman mountains. In: J. Malpas, E.M. Moores, A. Panayiotou and C. Xenophontos (Eds.), Ophiolites: Oceanic crustal analogues, Proc. Symposium "Troodos 1987". Geol. Surv. Dept., Ministry Agric. Nat. Res., Nicosia, Cyprus, 375-384.

Urquhart E. and Banner F.T., 1994. Biostratigraphy of the supra-ophiolite sediments of the Troodos Massif, Cyprus: the Cretaceous Perapedhi, Kannaviou, Moni and Kathikas formations. Geol. Mag., 131: 499-518.

Wagreich M., Bojar A.-V., Sachsenhofer R.F., Neuhuber S. and Egger H., 2008. Calcareous nannoplankton, planktonic foraminiferal, and carbonate carbon isotope stratigraphy of the Cenomanian-Turonian boundary section in the Ultrahelvetic Zone (Eastern Alps, Upper Austria). Creta. Res., 29: 965-975.

Warren C.J., Parrish R.R., Waters D.J. and Searle M.P., 2005. Dating the geologic history of Oman's Semail ophiolite: insights from U-Pb geochronology. Contrib. Mineral. Petrol., 150: 403-422.

Woodcock N.H. and Robertson A.H.F., 1982. Stratigraphy of the Mesozoic rocks above the Semail ophiolite, Oman. Geol. Mag., 119: 67-76.

Received, December 17, 2015
Accepted, December 15, 2016

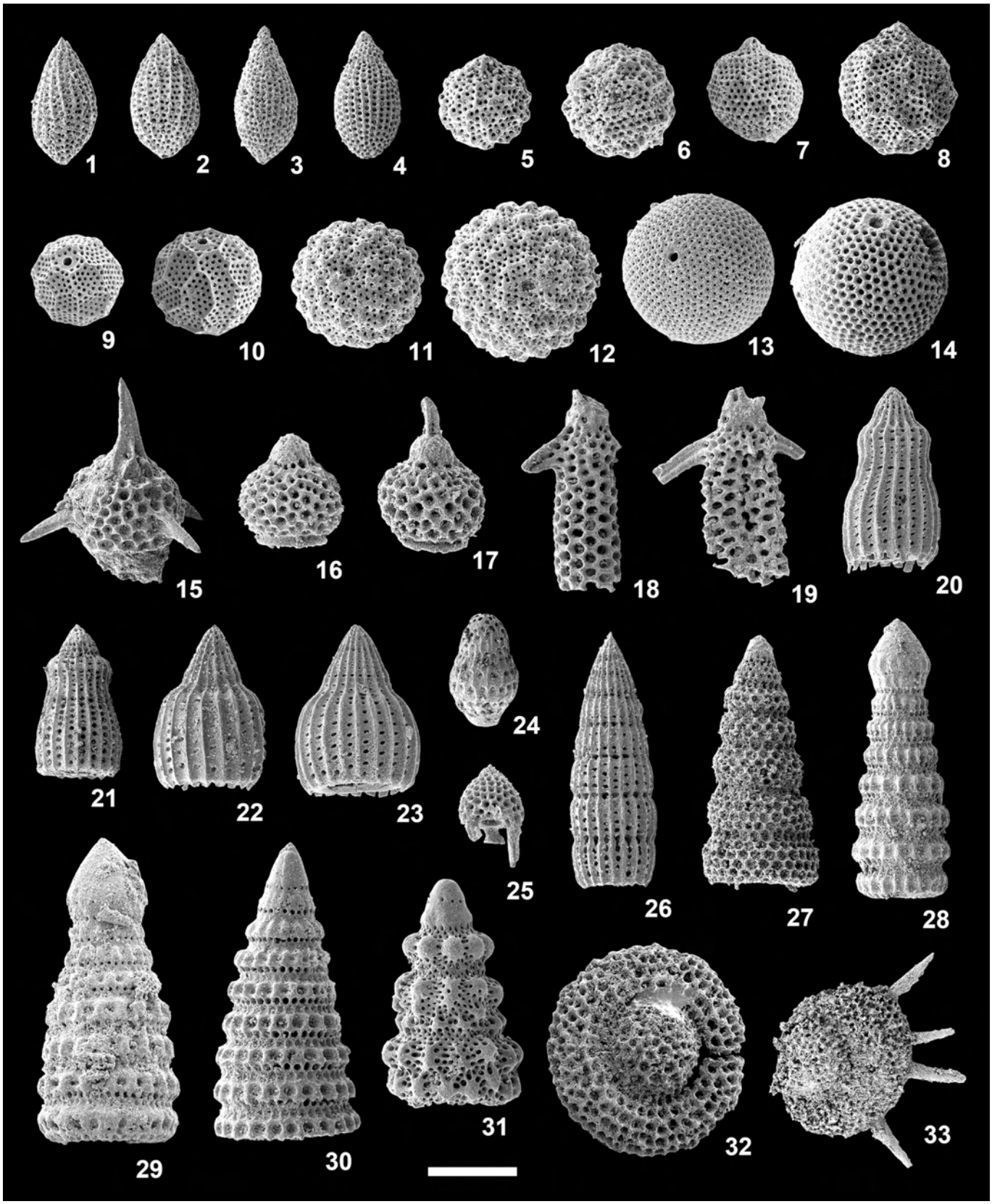

Plate 1 - (scale bar = 100 μm) 1, 2 - *Guttacapsa biacuta* (Squinabol), 1, E-03, 2, E0-370. 3, 4 - *Guttacapsa gutta* (Squinabol), 3, E-02, 4, E-03.5b. 5, 6 - *Hemicryptocapsa tuberosa* Dumitrica, 5, E-03.5b, 6, E0-210. 7, 8 - *Hemicryptocapsa prepolyhedra* Dumitrica, 7, E-02, 8, E-03.5b. 9, 10 - *Hemicryptocapsa polyhedra* Dumitrica, 9, C-08, 10, C-24. 11, 12 - *Holocryptocanium tuberculatum* Dumitrica, 11, E-02, 12, E0-370. 13 - *Holocryptocanium barbui* Dumitrica, E0-40. 14 - *Holocryptocanium* sp. A, E-03.5c. 15 - *Rhopalosyringium elegans* (Squinabol), E-02. 16, 17 - *Rhopalosyringium majuroense* Schaaf, 16, E0-370, 17, E-02. 18, 19 - *Rhopalosyringium petilum* (Foreman), 18, E-02, 19, E0-40. 20, 21 - *Thanarla veneta* (Squinabol), 20, E0-40, 21, E0-370. 22, 23 - *Thanarla pulchra* (Squinabol), 22, E0-370, 23, E0-40. 24 - *Pseudotheocampe* sp. A, E0-370. 25 - *Myllocercion* sp., E0-40. 26 - *Archaeodictyomitra montisserei* (Squinabol), E0-210. 27 - *Stichomitra communis* Squinabol, E0-210. 28, 29 - *Pseudodictyomitra pseudomacrocephala* (Squinabol), 28, E-03.5b, 29, C-28. 30 - *Pseudodictyomitra tiara* (Holmes), E-03.5c. 31 - *Novixitus mclaughlini* (Pessagno), E0-40. 32 - *Dactyliosphaera silviae* Squinabol, E0-210. 33) *Dactyliodiscus longispinus* (Squinabol), E0-370.

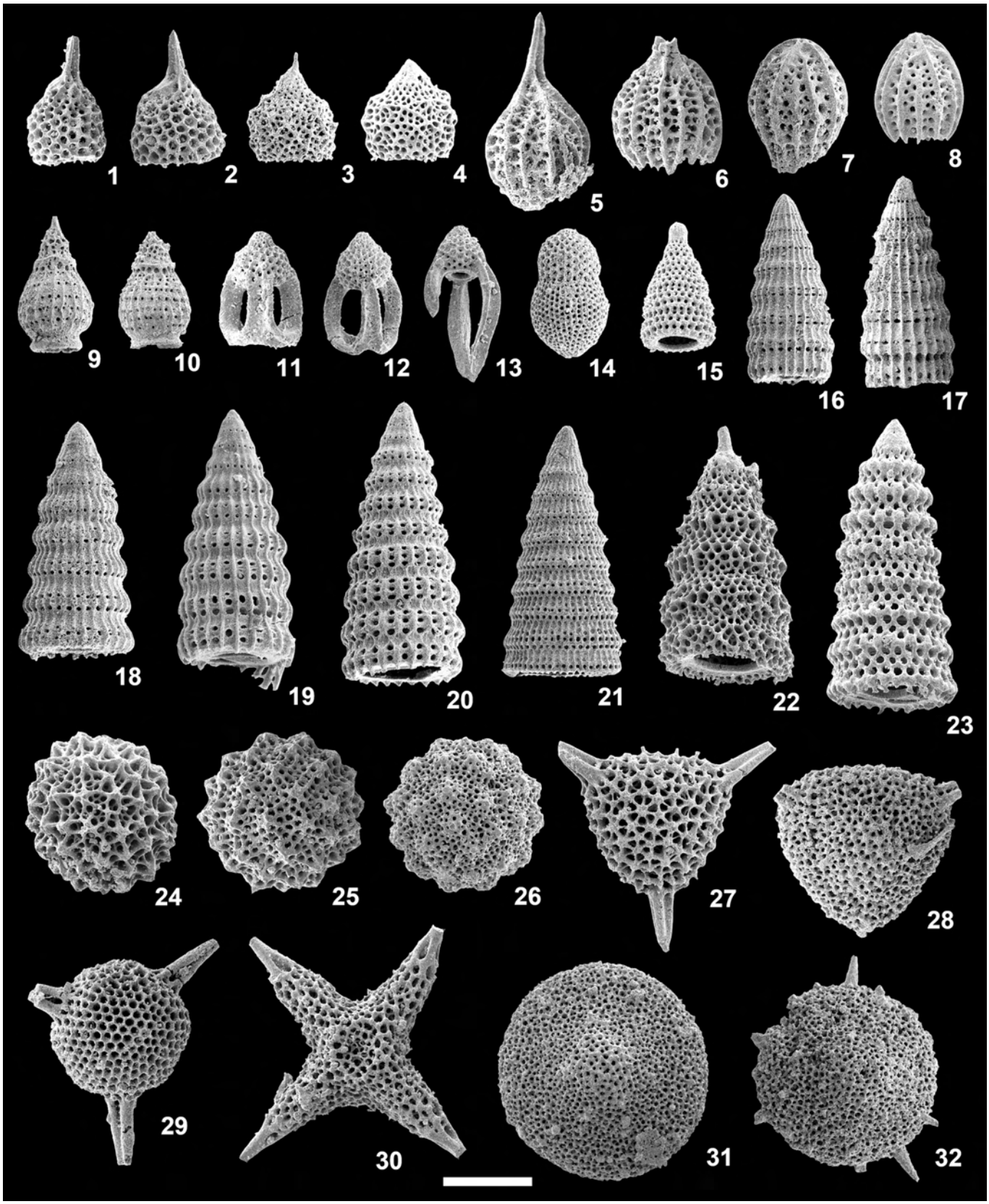

Plate 2 - (scale bar = 100 μm) 1, 2 - *Rhopalosyringium hispidum* O'Dogherty, 1, E-06, 2, A-25. 3, 4 - *Rhopalosyringium* sp. A, 3, A-15, 4, C-08. 5-8 - *Rhopalosyringium scissum* O'Dogherty, 5, E-03.5e, 6, C-24, 7, A-15, 8, C-07. 9, 10 - *Pseudotheocampe urna* (Foreman), 9, A-25, 10, C-24. 11, 12 - *Annikaella omanensis* De Wever, Bourdillon-de Grissac, and Beurrier, 11, C-24, 12, A-25. 13 - *Myllocercion valgus* (De Wever, Bourdillon-de Grissac, and Beurrier), C-24. 14 - *Diacanthocapsa ovoidea* Dumitrica, A-25. 15 - *Amphipternis* sp. cf. *A. stocki* (Campbell and Clark), C-14. 16, 17 - *Dictyomitra multicostata* Zittel, 16, A-13, 17, E-03.5c. 18, 19 - *Dictyomitra formosa* Squinabol, 18, A-13, 19, E-12. 20 - *Pseudodictyomitra* sp. A, A-11. 21 - *Pseudodictyomitra* sp. B, A-11. 22 - *Eostichomitra* sp. A, C-14. 23 - *Foremanina schona* Empson-Morin, C-07. 24 - *Praeconocaryomma californiaensis* Pessagno, C-07. 25 - *Praeconocaryomma universa* Pessagno, C-24. 26 - *Praeconocaryomma lipmanae* Pessagno, C-19. 27 - *Alievium superbum* (Squinabol), A-11. 28 - *Pseudoaulophacus putahensis* Pessagno, A-19. 29 - *Triactoma hexeris* O'Dogherty, A-15. 30 - *Crucella cachensis* Pessagno, C-24. 31 - *Patellula verteroensis* (Pessagno), C-24. 32 - *Patellula helios* (Squinabol), A-19.